Connectome Harmonic Decomposition of Human Brain Dynamics Reveals a Landscape of Consciousness

Luppi A.I. [a,b]*, Vohryzek J. [c,d], Kringelbach M. L.[c,d], Mediano P.A.M. [e], Craig M. M. [a,b], Adapa R. [a], Carhart-Harris, R. L. [f], Roseman, L. [f], Pappas I. [a,b,g], Finoia P. [a,h], Williams G. B. [b,i], Allanson J. [b,j], Pickard J. D. [b,h,i], Menon D. K. [a], Atasoy S. [c,d], & Stamatakis E.A. [a,b]

[a]Division of Anaesthesia, School of Clinical Medicine, University of Cambridge, Cambridge, United Kingdom

[b]Department of Clinical Neurosciences, University of Cambridge, Cambridge, United Kingdom

[c]Department of Psychiatry, University of Oxford, Oxford, United Kingdom

[d]Center for Music in the Brain, Aarhus University, Aarhus, Denmark

[e]Department of Psychology, University of Cambridge, Cambridge, United Kingdom

[f]Center for Psychedelic Research, Department of Brain Sciences, Imperial College London, London, United Kingdom

[g]Department of Psychology and Helen Wills Neuroscience Institute, University of California - Berkeley, Berkeley, California, USA

[h]Division of Neurosurgery, School of Clinical Medicine, University of Cambridge, Cambridge, United Kingdom

[i]Wolfson Brain Imaging Centre, University of Cambridge, Cambridge, United Kingdom

[j]Department of Neurosciences, Cambridge University Hospitals NHS Foundation, Addenbrooke's Hospital, Cambridge, United Kingdom

*Corresponding author: email al857@cam.ac.uk

ABSTRACT

A central question in neuroscience is how cognition and consciousness arise from human brain activity. Here, we decompose cortical dynamics of resting-state functional MRI into their constituent elements: the harmonics of the human connectome. Mapping a wide spectrum of consciousness onto these elementary brain states reveals a generalisable connectome harmonic signature of loss of consciousness, whether due to anaesthesia or severe brain injury. Remarkably, its mirror-reversed image corresponds to the harmonic signature of the psychedelic state induced by ketamine or LSD, identifying meaningful

relationships between neurobiology, brain function, and conscious experience. The repertoire of connectome harmonics further provides a fine-tuned indicator of level of consciousness, sensitive to differences in anaesthetic dose and clinically relevant sub-categories of patients with disorders of consciousness. Overall, we reveal that the emergence of consciousness from human brain dynamics follows the same universal principles shared by a multitude of physical and biological phenomena: the mathematics of harmonic modes.

MAIN TEXT

Relating subjective mental states to the underlying brain states remains a key challenge for contemporary neuroscience[1]. Despite recent advances, what remains elusive is a principled account of how the spatio-temporal brain dynamics that support consciousness[1–7], arise from the interplay of cortical dynamics across the brain's anatomical connections[8].

The emerging framework of connectome harmonic decomposition offers a way to bridge this gap, decomposing complex brain dynamics (derived e.g. from functional MRI) in terms of neurobiologically grounded, elementary brain states[8–11]. Just like human language can generate infinite meanings from recombination of a finite vocabulary, so the human brain can generate an endless variety of mental states, by recombining a finite set of neural building blocks. Mathematically, connectome harmonic decomposition (CHD) extends the well-known Fourier transform to the human brain[8]. Through the Fourier transform, any signal can be represented as a combination of fundamental sinusoids: the harmonic modes of a linear filter. Likewise, CHD decomposes any pattern of cortical activity into a set of universal basis functions of increasing spatial frequency (granularity): the harmonic modes of the human connectome[8]. Harmonic modes are ubiquitous across natural phenomena, ranging from acoustic vibrations and electron orbits, to animal coat patterns and

morphogenesis[12,13]. In the human brain, harmonic modes (termed connectome harmonics; though spherical harmonics have also been used[14]) emerge from the balance between neuronal excitation and inhibition interacting over anatomical connections[8,13]. Thus, CHD provides an avenue to decompose and compare brain dynamics across states of consciousness, in a way that is (i) universal across individuals, and (ii) grounded in brain anatomy and neurophysiology[8]: a shared vocabulary for the language of human brain activity, derived from fundamental mathematical principles. Here, we leverage the CHD framework to map the landscape of human consciousness, revealing how connectome harmonics orchestrate the emergence of different states of consciousness (Figure 1 and Supplementary Figure 1).

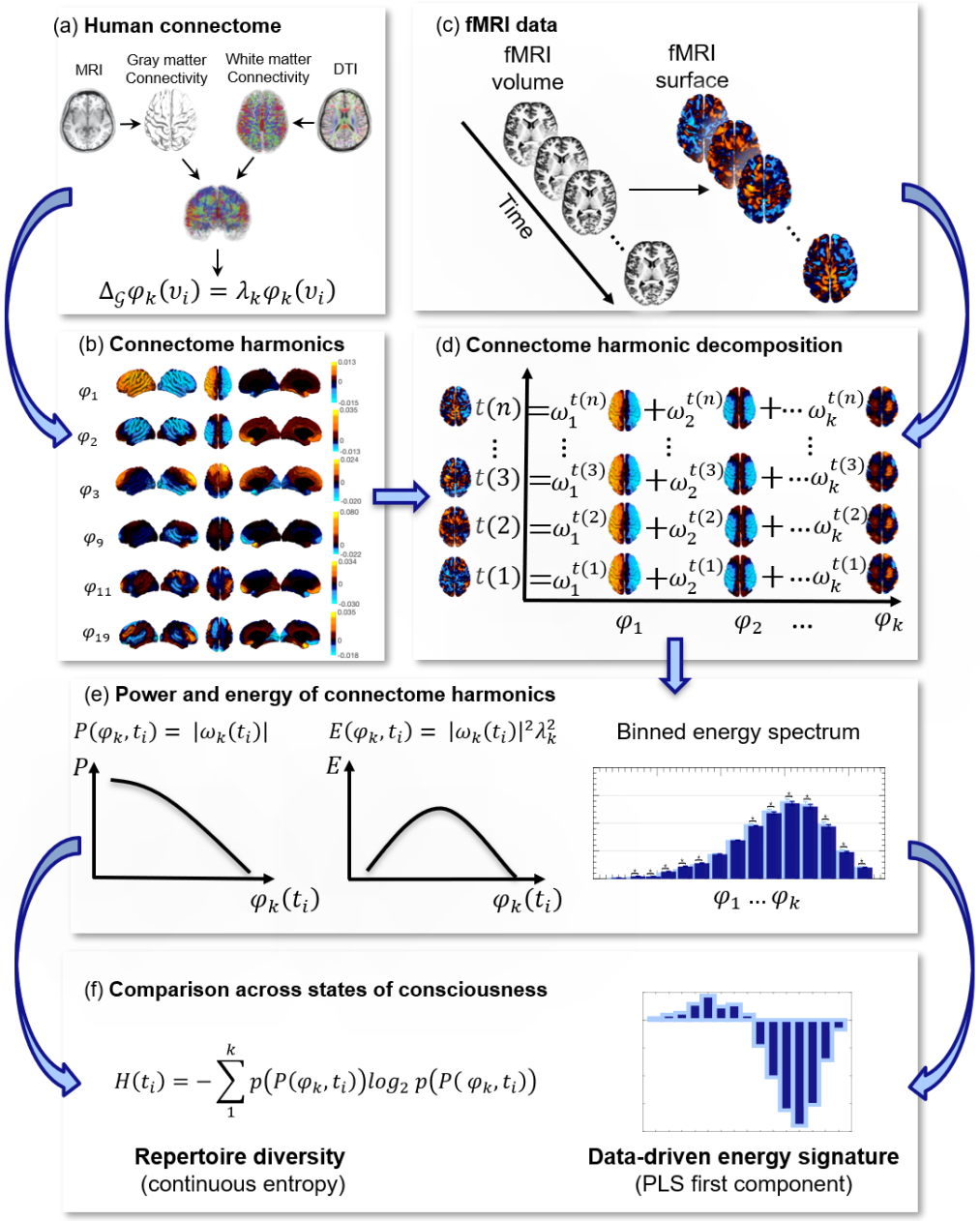

Figure 1. Overview of connectome harmonics analysis framework. (a) High-resolution rendering of the human connectome is achieved by reconstructing the surface-based grey matter computed from structural magnetic resonance imaging (sMRI) and the white-matter axonal tracts calculated with diffusion tensor imaging (DTI). (b) Connectome harmonics are obtained as the eigenvectors of the graph Laplacian applied to the human connectome. With an increasing connectome harmonic number k, we obtain more complex and fine-grained spatial patterns. (c) Volumetric functional magnetic resonance imaging (fMRI) data are projected onto the cortical surface for every timepoint t_i. (d) Connectome harmonic decomposition (CHD) of the fMRI data estimates the contribution $\omega_k(t_i)$ of individual harmonics φ_k to the cortical activity at every timepoint t_i. **Measures of the connectome harmonic spectrum.** (e) The power spectrum

is estimated as the absolute contribution $|\omega_k(t_i)|$ of individual harmonics φ_k to the fMRI data at every time point t_i. Similarly, the energy spectrum is estimated as the square of the absolute contribution $|\omega_k(t_i)|$ of individual harmonics φ_k to the fMRI data, weighted by the square of the harmonics' corresponding eigenvalue λ_k at every time point t_i. The overall binned energy spectrum across subjects and timepoints is constructed by discretising the energy of connectome harmonics in 15 logarithmically-spaced frequency-specific bins, here shown for a target state (dark blue) and a reference state (light blue). (f) Repertoire entropy is defined as the entropy of the power spectrum at every timepoint t_i, computed with the continuous Kozachenko approximation; the data-driven energy signature of a target state of consciousness is obtained from the first principal component of Partial Least Squares-Discriminant Analysis (PLS-DA), which maximally discriminates the target state (dark blue) from the reference state (light blue), based on their respective connectome harmonic energy spectra.

Connectome harmonic signatures of consciousness

Previous work has shown that CHD can identify consistent signatures of the psychedelic state induced by the serotonin $5HT_{2A}$ receptor agonists LSD and psilocybin, in terms of a shift in energy (normalised contribution) from low- to high-frequency harmonics, corresponding to increasingly complex neural dynamics[8–10]. The psychedelic state has been postulated to represent one end of the spectrum of conscious states[15,16], with loss of consciousness at the opposite end, in terms of subjective experience as well as observable effects on brain function and dynamics[7,17–21] (however, see Bayne and Carter (2018)[22]). To map the complete spectrum of consciousness, we therefore investigated resting-state functional MRI (rs-fMRI) data from volunteers undergoing sedation with the intravenous anaesthetic, propofol[23] (N=15). As an agonist of the chief inhibitory neurotransmitter GABA, propofol enhances the activity of inhibitory interneurons, leading to globally increased neuronal inhibition[24]. Computational modelling has previously demonstrated that a shift in energy from high- to low-frequency harmonics (i.e. the opposite of what is observed with LSD and psilocybin[8–10]) can arise from reduced global excitation or increased global inhibition[8,13]. Therefore, computational and theoretical reasons converge to predict that propofol should induce connectome harmonic alterations that are the opposite of what is observed with psychedelics.

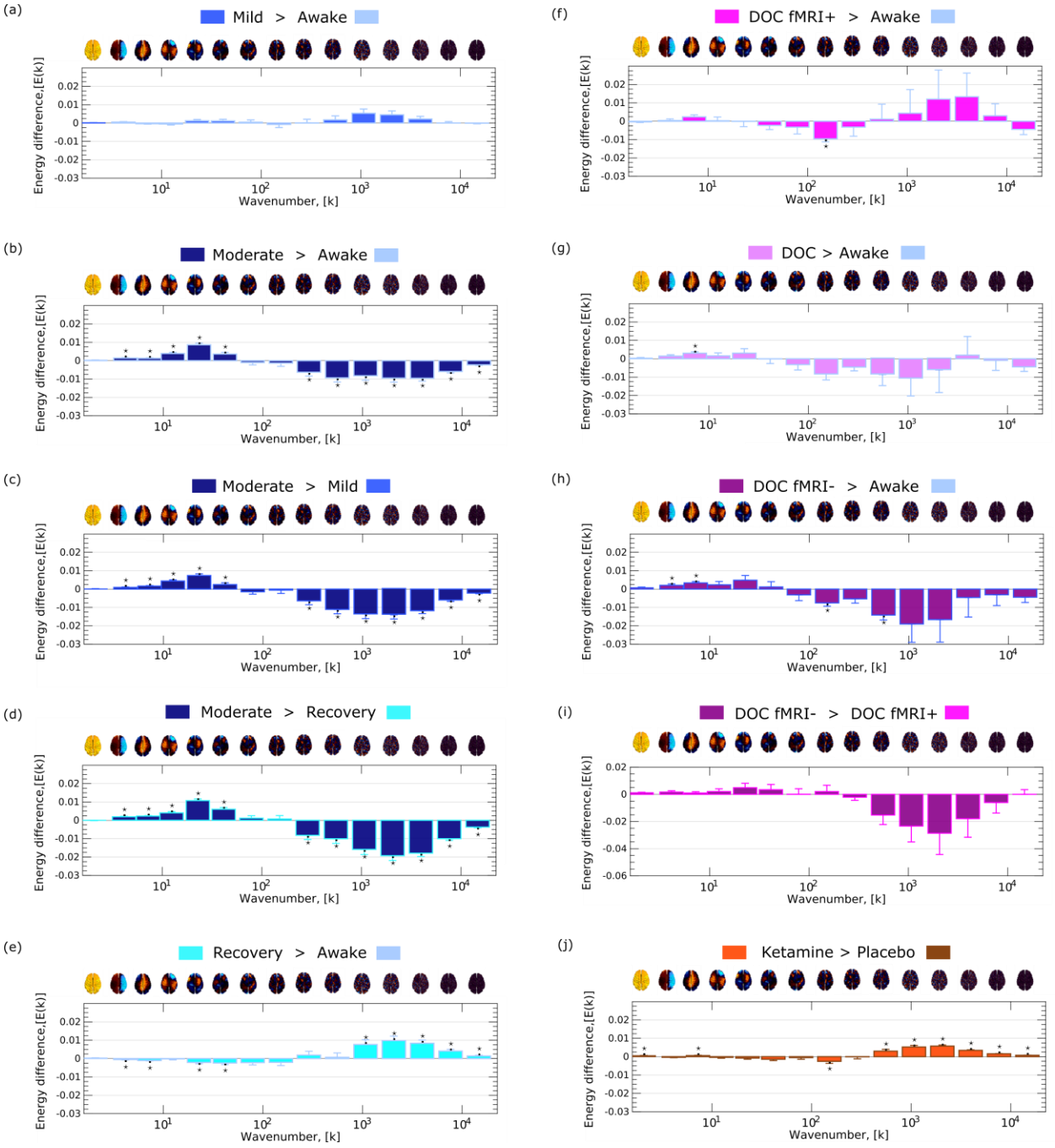

Figure 2. **Frequency-specific energy changes across states of consciousness.** (a) Mild propofol sedation > wakefulness. (b) Moderate anaesthesia > wakefulness. (c) Moderate anaesthesia > mild sedation. (d) Moderate anaesthesia > post-anaesthetic recovery. (e) Recovery > wakefulness. (f) DOC patients > awake healthy controls. (g) DOC fMRI+ patients > awake healthy controls. (h) DOC fMRI- patients > awake healthy controls. (i) fMRI- > fMRI+ DOC patients. (j) Ketamine > placebo. * $p < 0.05$, FDR-corrected across 15 frequency bins. A brain surface projection of the connectome harmonic pattern corresponding to each frequency bin, averaged over the constituent spatial frequencies, is shown above each bin.

To further establish whether the connectome harmonic signature of anaesthesia is representative of other ways of losing consciousness, we also considered a cohort of N=22 patients diagnosed with chronic disorders of consciousness arising from severe brain injury[3]. We investigated whether CHD could detect consciousness in a subset of patients who had previously exhibited evidence of covert consciousness by performing mental imagery tasks in the scanner[25,26] (in terms of specific brain regions activating when patients were asked to imagine playing tennis or navigating around their house) (fMRI+; N=8), compared with patients who had provided no such evidence (fMRI-; N=14).

Our results reveal a general connectome harmonic signature of loss of consciousness across anaesthesia and disorders of consciousness (Figure 2, Supplementary Figure 2 and Supplementary Table 1), characterised by a shift in the energy distribution from high to low-frequency harmonic modes - the opposite of the pattern previously observed with psychedelics[9,10]. These characteristic alterations of connectome harmonic energy are specific to loss of consciousness. Firstly, no significant energy alterations of the connectome harmonic spectrum are observed during a lower dose of propofol administration (mild sedation), when participants are still conscious. Instead, significant alterations are only observed during moderate anaesthesia, once participants have lost responsiveness. Secondly, the pattern observed during moderate anaesthesia is reversed upon awakening. Thirdly, the same connectome harmonic signature is also observed for chronic loss of consciousness induced by severe brain injury. A shift in energy from high to low frequencies was found when comparing controls with unconscious (fMRI-) DOC patients, with a similar trend also being evident when comparing the sub-groups of fMRI- and fMRI+ (covertly conscious) DOC patients. Finally, this putative unconsciousness-specific pattern of connectome harmonic energy was *not* observed when comparing fMRI+ DOC patients with awake volunteers – as we should expect from a specific marker of unconsciousness, given that each fMRI+ patient had previously provided evidence of being covertly conscious.

Intriguingly, the opposite pattern (elevated energy in high-frequency connectome harmonics, and reduced energy in low-frequency ones) was observed when comparing post-anaesthetic recovery and pre-anaesthetic wakefulness – resembling the pattern previously observed with classic psychedelics[9,10]. Extending the Wilson-Cowan neural model to the human connectome, Atasoy and colleagues[8] have previously demonstrated that high-frequency harmonics emerge when excitation is increased, or inhibition is diminished. Recovery from anaesthesia corresponds to a gradual reduction of the (abnormally high) global inhibition induced by propofol. Thus, the resulting effects on the energy distribution should be the same as those observed when increasing global excitation (e.g. due to ketamine or LSD infusion), which is remarkably, precisely what we observed here. Though speculative, this account may explain the well-known phenomenon whereby individuals emerging from anaesthesia can exhibit symptoms of delirium, cognitive alterations, and even hallucinations[27,28]. Thus, our observed similarity between anaesthetic emergence and psychedelics may provide a link between physiology (reduced neuronal inhibition due to diminished levels of anaesthetic) and its corresponding cognitive manifestation.

Having established that the connectome harmonic signature of loss of consciousness is the same regardless of its cause, we investigated whether connectome harmonics could also reveal a general signature of the psychedelic state. We reasoned that if the pattern of connectome harmonic alterations induced by the serotonergic psychedelics LSD and psilocybin[9,10] represents a general signature of the psychedelic state, then the same connectome harmonic signature should also be observed during psychedelic experiences induced by drugs that operate through different molecular mechanisms. We investigated this hypothesis with rs-fMRI data from N=20 volunteers undergoing infusion with a psychoactive (sub-anaesthetic) dose of the N-methyl-D-aspartate receptor antagonist ketamine[29,30], which induces dissociative symptoms and is considered to be a useful model of psychosis[29,31] (although see[32]). Our results revealed an increase in the energy of high-frequency harmonics, analogous to that induced by LSD and psilocybin[9,10].

The gradient from low- to high-frequency connectome harmonics reflects progressive decoupling of the corresponding neural activity from the underlying structural connectivity[33]. Thus, the psychedelic-induced energy shift to high-frequency harmonics indicates a departure from standard activity patterns encoded in the structural connectome, in favour of increasingly diverse ones - a plausible neural correlate for the phenomenologically rich state of mind induced by psychedelics[8–10].

Generalisability and predictive power of connectome harmonic signatures across states of consciousness

The emergence of two mirror-reversed patterns of connectome harmonic energy, one for unconsciousness (whether due to anaesthesia or severe brain injury) and one for the psychedelic state (whether induced by ketamine or serotonergic psychedelics[9,10]), suggests that it should be possible to generalise these patterns across datasets to establish the harmonic signature of a) unconsciousness and b) psychedelic experience.

To pursue this hypothesis, we applied a data-driven technique known as Partial Least Squares - Discriminant Analysis (PLS-DA)[34], to extract the multivariate pattern of connectome harmonic energy that maximally distinguished between each pair of conditions (termed multivariate signature, MVS; Supplementary Figure 3). We then projected each subject's energy spectrum onto the MVS characterising a given state of consciousness, to quantify their similarity (Methods). To investigate the generalisability of the connectome harmonic signature of ketamine to other psychedelics, the LSD data previously used by Atasoy and colleagues[9,10] were also included in this new analysis.

Supporting the notion that two mirror-reversed patterns characterise loss of consciousness and the psychedelic state, this analysis revealed similar projections for the multivariate

signatures (MVS) extracted from propofol anaesthesia (moderate vs awake) and from DOC patients (fMRI- vs fMRI+), which were opposite of the projections onto ketamine (vs placebo) and onto LSD (vs placebo) (Supplementary Figure 4 and Supplementary Table 2). The observation that loss of consciousness and the psychedelic state have diametrically opposite harmonic signatures, also lends support for the intriguing possibility of employing psychedelics to treat disorders of consciousness[35].

As an even more compelling demonstration that the signatures of unconsciousness extracted from CHD are truly generalisable across ways of losing consciousness, we show that individuals undergoing greater changes in propofol plasma concentration levels when transitioning from consciousness to unconsciousness and back, also exhibit larger differences in their correspondence to the harmonic pattern that discriminates between covertly conscious and unconscious DOC patients.

Specifically, the propofol-induced change in fMRI projection score onto the multivariate energy signature extracted from DOC patients, was significantly correlated with the change in serum propofol levels when transitioning from mild to moderate propofol anaesthesia (Spearman's ρ = 0.57, $CI_{95\%}$ [0.08, 0.84], p = 0.026; Figure 3a). Likewise, the change in projection score onto the DOC MVS also predicted the change in serum propofol levels between moderate sedation and post-anaesthetic recovery (Spearman's ρ = 0.56, $CI_{95\%}$ [0.07, 0.83], p = 0.030; Figure 3b).

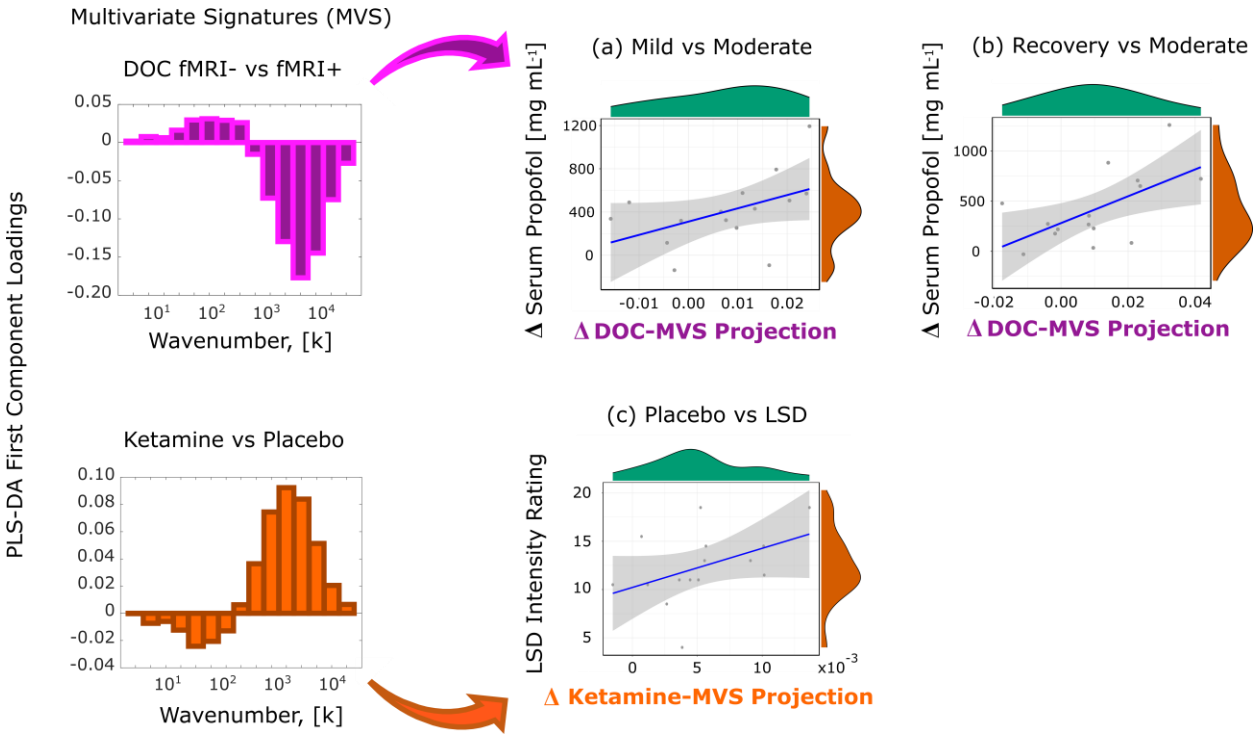

Figure 3. Projection onto cross-dataset multivariate energy signatures (MVS) correlate with propofol levels between consciousness and unconsciousness, and subjective intensity of the LSD experience. (a) Scatterplot of the change (moderate anaesthesia minus mild) in connectome harmonic energy projection onto the multivariate energy signature (MVS) derived from the DOC dataset, versus the change in propofol levels in volunteers' blood serum, between mild and moderate propofol anaesthesia. (b) Scatterplot of the change (moderate minus recovery) in connectome harmonic energy projection onto the multivariate signature derived from the DOC dataset, versus the change in propofol levels in volunteers' blood serum, between moderate anaesthesia and recovery. (c) Scatterplot of the change (LSD minus placebo) in connectome harmonic energy projection onto the multivariate signature derived from the ketamine dataset, versus the subjective intensity of the psychedelic experience induced by LSD.

Furthermore, generalisability of connectome harmonic signatures also extends to the psychedelic state: the subjective intensity of the psychedelic experience induced by LSD, was predicted by the LSD-induced change in projection score onto the multivariate signature derived from ketamine (Spearman's $\rho = 0.57$, $CI_{95\%}$ [0.08, 0.84], $p = 0.026$; Figure 3c). Importantly, the same MVS projections were not significantly correlated with differences in subject motion, for both the propofol and LSD datasets, thereby excluding a potential confound (Supplementary Table 3 and Supplementary Figure 5). These findings identify general connectome harmonic signatures of conscious-to-unconscious transitions (and vice a versa) induced by both propofol anaesthesia and DOC, as well as general

signatures of the psychedelic experience, relating neural dynamics to subjective phenomenology.

Repertoire diversity of connectome harmonics tracks level of consciousness

Finally, we investigated whether the diversity of mental experiences during a given state of consciousness can be quantified in terms of diversity of connectome harmonic patterns contributing to brain activity – the central tenet of recent theoretical efforts seeking to establish a correspondence between the dynamics of mind and brain[1,15].

We therefore quantified the diversity of the distribution of harmonic power (absolute magnitude of contribution) at each timepoint by means of the entropy of that distribution. The higher the value of this measure, which we term "harmonic repertoire diversity", the wider the range of connectome harmonics that are recruited to compose cortical activity. Thus, states of diminished consciousness, where the diversity of mental content is limited, should be characterised by reduced entropy of the connectome harmonic repertoire, reflecting a more restricted repertoire of brain patterns. Conversely, increased repertoire diversity should be observed with ketamine and LSD, reflecting the high diversity of experiences occurring in the psychedelic state[15,16].

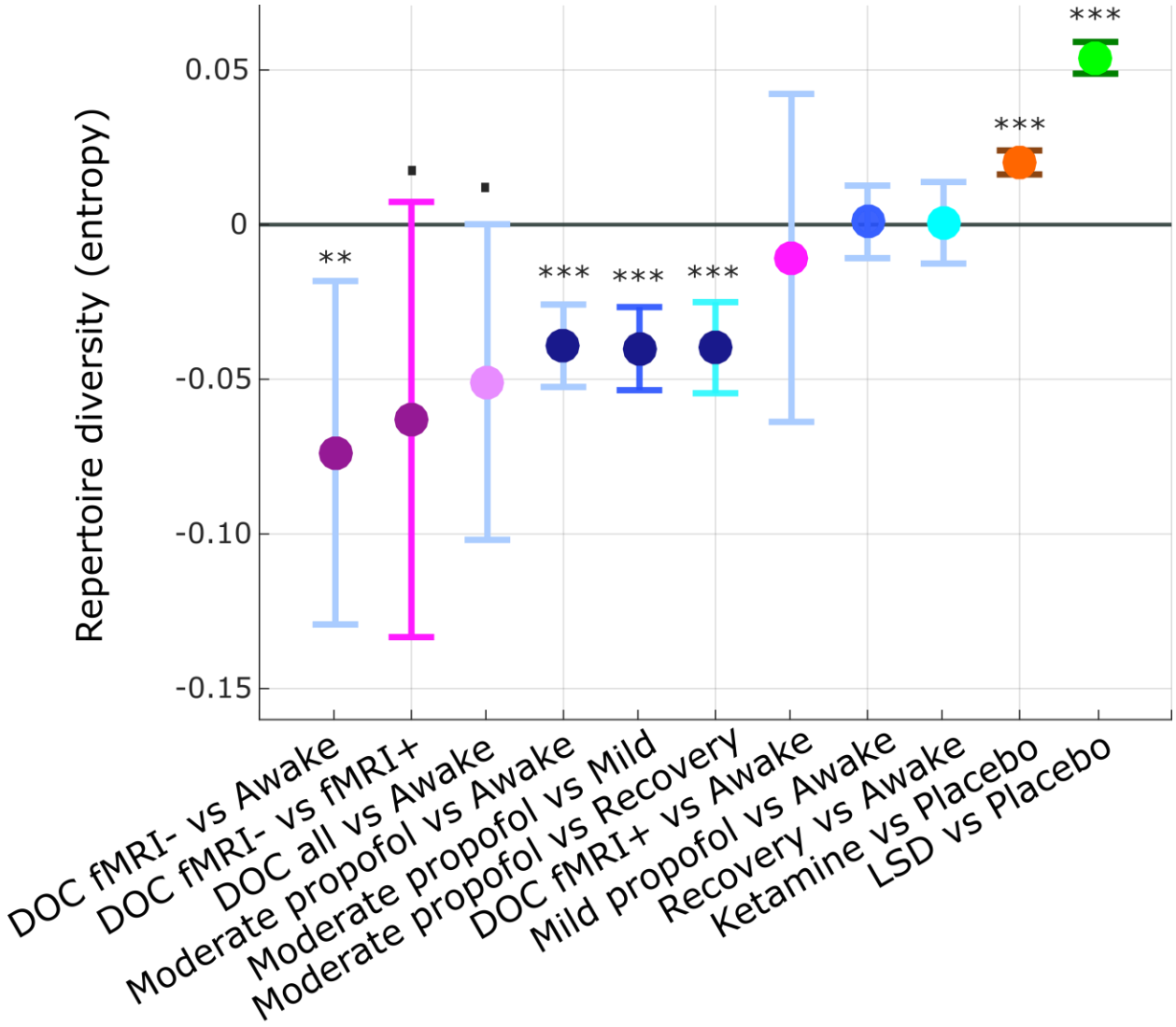

Figure 4. Diversity of connectome harmonic repertoire tracks level of consciousness from loss of responsiveness to psychedelics. Fixed effects (and 95% CI) of the comparison in repertoire diversity (entropy of connectome harmonic power distribution) between pairs of conditions (states of consciousness), treating condition as a fixed effect, and subjects as random effects. Timepoints were also included as random effects, nested within subjects. *** $p < 0.001$; ** $p < 0.01$; . $p < 0.10$.

Our results support both of these predictions (Supplementary Table 4 and Figure 4). Ketamine and LSD exhibited significantly higher diversity of the repertoire of connectome harmonics than placebo, whereas moderate anaesthesia with propofol resulted in reduced diversity when compared with wakefulness, recovery, and even mild sedation. Conversely, neither of the latter conditions (during which volunteers were conscious) was significantly different from normal wakefulness in terms of their diversity of harmonic repertoire,

despite the presence of propofol in the blood in both cases - thereby indicating that diversity of the connectome harmonic repertoire tracks the level of consciousness rather than the mere presence of propofol.

Remarkably, our analysis revealed that DOC patients who had previously exhibited evidence of covert consciousness (fMRI+), also exhibited entropy levels approaching those of awake volunteers – in sharp contrast with fMRI- patients, who had provided no evidence of being conscious, and whose repertoire entropy was significantly compromised (Figure 4 and Supplementary Table 3). Thus, our results demonstrate that the diversity of connectome harmonic repertoire (measured in terms of entropy) can track level of consciousness on a one-dimensional scale.

Although our results pertaining to DOC patients consistently followed the same pattern as moderate anaesthesia, they sometimes narrowly failed to reach statistical significance due to the large variability among patients - which is hardly unexpected since DOC are highly heterogeneous conditions, varying in the source, location and extent of brain damage. Although these results warrant caution until replicated in a different dataset, none of our conclusions rest solely on the results from the DOC dataset. We also acknowledge that loss of behavioural responsiveness during anaesthesia may not always coincide with loss of brain responsiveness and subjective experience[36–38], and even failure to respond to the fMRI mental imagery tasks cannot conclusively rule out residual consciousness in DOC patients: future research may benefit from seeking convergence across different task-free neural correlates of consciousness[37,39,40].

Nevertheless, it is noteworthy that although we stratified our DOC patients based on their performance on mental imagery tasks in the scanner, our connectome harmonic analysis was entirely based on resting-state (i.e., task-free) fMRI data, which imposes no cognitive demands on patients, unlike task-based paradigms[39]. Therefore, connectome harmonics analysis of re-fMRI may represent a useful screening tool in the clinic to identify patients

who may be covertly conscious – contributing to alleviate the high rate of misdiagnoses for DOC patients when relying solely on behavioural criteria[39], while demonstrating the potential clinical value of CHD as a general neural marker of consciousness bypassing overt behaviour.

Connectome harmonics as a framework to characterise conscious states

Across multiple datasets, we demonstrate that the emergence of consciousness from human brain dynamics follows the same universal principles shared by a multitude of physical and biological phenomena across scales: the mathematics of harmonic modes. Diversity of the connectome harmonic repertoire can provide a useful one-dimensional indicator of level of consciousness, sensitive to differences in anaesthetic dose (mild sedation vs moderate anaesthesia vs recovery) as well as sub-categories of patients with disorders of consciousness. Being grounded in the brain's anatomy and neurophysiology, connectome harmonics provide a mathematically principled explanatory framework to understand the loss of complexity that accompanies loss of consciousness. Namely, the collapse in the connectome harmonic repertoire reported here may constitute the link between neurobiology (propofol-induced global inhibition) and phenomenology (loss of subjective experience, i.e. unconsciousness) by restricting the set of states available to the brain.

Yet, connectome harmonics offer a richer characterisation of conscious states that goes beyond simple (though effective) complexity measures: the specific distribution of energy over connectome harmonics may be used to characterise the quality of various states of consciousness, in terms of being "unconscious-like" or "psychedelic-like" (or neither). Indeed, our analyses uncovered that the connectome harmonic signature of post-anaesthetic recovery (and, to a lesser extent, mild sedation), resembled the signature of the psychedelic state– even though diversity of the repertoire was near baseline levels.

Thus, composition of the energy spectrum and diversity of the harmonic repertoire provide distinct and synergistic insights to identify meaningful relationships between brain function and conscious experience. Having demonstrated its power and generalisability across datasets and states of consciousness, the framework of connectome harmonic decomposition may be especially useful in the characterisation of a wider set of mental states, from dreaming to psychosis.

MATERIALS AND METHODS

Ketamine Dataset

Recruitment

A total of 21 participants (10 males; mean age 28.7 years, SD = 3.2 years) were recruited via advertisements placed throughout central Cambridge, UK. All participants underwent a screening interview in which they were asked whether they had previously been diagnosed or treated for any mental health problems and whether they had ever taken any psychotropic medications. Participants reporting a personal history of any mental health problems or a history of any treatment were excluded from the study. All participants were right-handed, were free of current of previous psychiatric or neurological disorder or substance abuse problems, and had no history of cardiovascular illness or family history of psychiatric disorder/substance abuse. The study was approved by the Cambridge Local Research and Ethics Committee, and all participants provided written informed consent in accordance with ethics committee guidelines. The acquisition and design are described in detail in a previous study [29].

Study Design

Participants were assessed on two occasions, separated by at least 1 week. On one occasion, they received a continuous computer-controlled intravenous infusion of a racemic ketamine solution (2 mg/ml) until a targeted plasma concentration of 100 ng/ml was reached. This concentration

was sustained throughout the protocol. A saline infusion was administered on the other occasion. Infusion order was randomly counterbalanced across participants. The infusion was performed and monitored by a trained anesthetist (RA) who was unblinded for safety reasons, but who otherwise had minimal contact with participants. At all other times, participants were supervised by investigators blinded to the infusion protocol. The participants remained blinded until both assessments were completed. All MRI and assessment procedures were identical across assessment occasions.

Infusion Protocol

Bilateral intravenous catheters were inserted into volunteers' forearms, one for infusion, and the other for serial blood sampling. We used a validated and previously implemented [41] three-compartment pharmacokinetic model to achieve a constant plasma concentration of 100 ng/ml using a computerized pump (Graseby 3500, Graseby Medical, UK). The infusion continued for 15 min to allow stabilization of plasma levels. Blood samples were drawn before and after the resting fMRI scan and then placed on ice. Plasma was obtained by centrifugation and stored at −70 °C. Plasma ketamine concentrations were measured by gas chromatography–mass spectrometry.

MRI Acquisition

Scanning was performed using a 3.0 T MRI scanner (Siemens Magnetom, Trio Tim, Erlangen, Germany) equipped with a 12-channel array coil located at the Wolfson Brain Imaging Centre, Addenbrooke's Hospital, Cambridge, UK. T2*-weighted echo-planar images were acquired under eyes-closed resting-state conditions. Participants were instructed to close their eyes and let the minds wander without going to sleep. Subsequent participant debriefing ensured that no participants fell asleep during the scan. Imaging parameters were: 3x3x3.75mm voxel size, with a time-to-repetition (TR) of 2000 ms, time-to-echo (TE) of 30 ms, flip angle of 781 in 64x64 matrix size, and 240mm field of view (FOV). A total of 300 volumes comprising 32 slices each were obtained. In addition, high- resolution anatomical T1 images were acquired using a three-dimensional magnetic-prepared rapid gradient echo (MPPRAGE) sequence. In all, 176 contiguous sagittal slices of 1.0mm thickness using a TR of 2300 ms, TE of 2.98 ms, flip angle of 91, and a FOV of 256mm in 240x256 matrix were acquired with a voxel size of 1.0mm^3. One participant was excluded due to excessive movement, resulting in a final sample of N=20 subjects.

Preprocessing

We preprocessed the functional imaging data using a standard pipeline, implemented within the SPM12-based (http://www.fil.ion.ucl.ac.uk/spm) toolbox CONN (http://www.nitrc.org/projects/conn), version 17f [42]. The pipeline comprised the following steps: removal of the first five scans, to allow magnetisation to reach steady state; functional realignment and motion correction; slice-timing correction to account for differences in time of acquisition between slices; identification of outlier scans for subsequent regression by means of the quality assurance/artifact rejection software *art* (http://www.nitrc.org/projects/artifact_detect); spatial normalisation to Montreal Neurological Institute (MNI-152) standard space with 2mm isotropic resampling resolution, using the segmented grey matter image from each volunteer's high-resolution T1-weighted image, together with an *a priori* grey matter template.

Denoising

To reduce noise due to cardiac and motion artifacts, we applied the anatomical CompCor method of denoising the functional data [43], also implemented within the CONN toolbox. The anatomical CompCor method involves regressing out of the functional data the following confounding effects: the first five principal components attributable to each individual's white matter signal, and the first five components attributable to individual cerebrospinal fluid (CSF) signal; six subject-specific realignment parameters (three translations and three rotations) as well as their first- order temporal derivatives; the artifacts identified by *art;* and main effect of scanning condition[43]. Linear detrending was also applied, and the subject-specific denoised BOLD signal timeseries were band-pass filtered to eliminate both low-frequency drift effects and high-frequency noise, thus retaining temporal frequencies between 0.008 and 0.09 Hz. Importantly, note that this bandpass filtering pertains to temporal frequencies, which are distinct from the spatial frequencies obtained from connectome harmonic decomposition (as described below).

Propofol Dataset

Recruitment

Ethical approval for these studies was obtained from the Cambridgeshire 2 Regional Ethics Committee, and all subjects gave informed consent to participate in the study. Sixteen healthy volunteer subjects were recruited for scanning. The acquisition procedures are described in detail in a previous study [23]. In addition to the original 16 volunteers, data were acquired for nine additional participants using the same procedures, bringing the total number of participants in this dataset to 25 (11 males, 14 females; mean age 34.7 years, SD = 9.0 years).

Propofol Infusion Protocol

The GABA-ergic intravenous agent propofol is one of the most commonly used anaesthetic drugs, owing to the stability and predictability of its effects. Propofol was administered intravenously as a "target controlled infusion" (plasma concentration mode), using an Alaris PK infusion pump (Carefusion, Basingstoke, UK). Three target plasma levels were used - no drug (baseline), 0.6 mg/ml (mild sedation) and 1.2 mg/ml (moderate sedation).

A period of 10 min was allowed for equilibration of plasma and effect-site propofol concentrations. Blood samples were drawn towards the end of each titration period and before the plasma target was altered, to assess plasma propofol levels. In total, 6 blood samples were drawn during the study. The mean (SD) measured plasma propofol concentration was 304.8 (141.1) ng/ml during mild sedation, 723.3 (320.5) ng/ml during moderate sedation and 275.8 (75.42) ng/ml during recovery. Mean (SD) total mass of propofol administered was 210.15 (33.17) mg, equivalent to 3.0 (0.47) mg/kg. The level of sedation was assessed verbally immediately before and after each of the scanning runs. The three conditions from this dataset are referred to as Awake, Mild and Moderate sedation respectively. Two senior anaesthetists were present during scanning sessions and observed the subjects throughout the study from the MRI control room and on a video link that showed the subject in the scanner. Electrocardiography and pulse oximetry were performed continuously, and measurements of heart rate, non-invasive blood pressure, and oxygen saturation were recorded at regular intervals.

FMRI Data Acquisition

The acquisition procedures are described in detail in the original study [23]. Briefly, MRI data were acquired on a Siemens Trio 3T scanner (WBIC, Cambridge). Each functional BOLD volume consisted of 32 interleaved, descending, oblique axial slices, 3 mm thick with interslice gap of 0.75 mm and in-plane resolution of 3 mm, field of view = 192x192 mm, repetition time = 2 s, acquisition time = 2 s, time echo = 30 ms, and flip angle 78. We also acquired T1-weighted structural images at 1 mm isotropic resolution in the sagittal plane, using an MPRAGE sequence with TR = 2250 ms, TI = 900 ms, TE = 2.99 ms and flip angle = 9 degrees, for localization purposes. Of the 25 healthy subjects, 15 were ultimately retained (7 males, 8 females): 10 were excluded, either because of missing scans (n=2), or due of excessive motion in the scanner (n=8, 5mm maximum motion threshold).

Preprocessing and Denoising

The same preprocessing and denoising procedures were followed as for the ketamine data.

Disorders of Consciousness Patient Dataset

Recruitment

A sample of 71 DOC patients was included in this study. Patients were referred from specialist rehabilitation settings as well as specialist nursing homes specifically identified in the ethics. All patients had been seen by a consultant neurologist or rehabilitation consultant before referral, to make diagnosis as part of multidisciplinary assessments. To be included in the study, patients must have had a DOC diagnosis, written informed consent to participation from their legal representative as well as the consent of their treating physician, and they must be capable of being transported to Addenbrooke's Hospital. The exclusion criteria included any medical condition that made it unsafe for the patient to participate (decision made by clinical personnel blinded to the specific aims of the study) or any reason they are unsuitable to enter the MRI scanner environment (e.g. non-MRI-safe implants), significant pre-existing mental health problems, or insufficient English pre injury. After admission to Addenbrooke’s Hospital, each patient underwent clinical neurological and neuroimaging testing, with pre-MRI CT for shunt management if needed. Patients spent a total of five days (including arrival and departure days) at Addenbrooke's Hospital.

Coma Recovery Scale-Revised (CRS-R) assessments were recorded at least daily for the five days of admission. If behaviours were indicative of awareness at any time, patients were classified as MCS; otherwise UWS. We assigned MCS- or MCS+ sub-classification if behaviours were consistent throughout the week. The most frequent signs of consciousness in MCS- patients are visual fixation and pursuit, automatic motor reactions (e.g. scratching, pulling the bed sheet) and localisation to noxious stimulation whereas MCS+ patients can, in addition, follow simple commands, intelligibly verbalise or intentionally communicate[44,45]. Scanning occurred at the Wolfson Brain Imaging Centre, Addenbrooke's Hospital, between January 2010 and December 2015; medication prescribed to each patient was maintained during scanning. Ethical approval for testing patients was provided by the National Research Ethics Service (National Health Service, UK; LREC reference 99/391). All clinical investigations were conducted in accordance with the Declaration of Helsinki.

As a focus of this study was on graph-theoretical properties of the brain, patients were systematically excluded from the final cohort analysed in this study based on the following criteria: 1) large focal brain damage (i.e. more than 1/3 of one hemisphere) as stated by an expert in neuroanatomy blinded to the patients' diagnoses; 2) excessive head motion during resting state scanning (i.e. greater than 3mm in translation and/or 3 degrees in rotation); 3) suboptimal segmentation and normalization of images. A total of 22 adults (14 males, 8 females; age range 17-70 years; mean time post injury: 13 months) meeting diagnostic criteria for Unresponsive Wakefulness Syndrome/Vegetative State (N = 10) or Minimally Conscious State (N = 12) due to brain injury were included in this study (Table 1).

Table 1: Demographic information for patients with Disorders of Consciousness.

Sex	Age	Months post injury	Aetiology	Diagnosis	CRS-R Score	Tennis	Spat Nav	Classification
M	46	23	TBI	UWS	6	no evidence	no evidence	fMRI-
M	57	14	TBI	MCS-	12	no evidence	no evidence	fMRI-
M	46	4	TBI	MCS	10	no evidence	no evidence	fMRI-
M	35	34	Anoxic	UWS	8	no evidence	no evidence	fMRI-
M	17	17	Anoxic	UWS	8	no evidence	positive	fMRI+
F	31	9	Anoxic	MCS-	10	no evidence	no evidence	fMRI-
F	38	13	TBI	MCS	11	positive	no evidence	fMRI+

M	29	68	TBI	MCS	10	SMA +ve	PPA +ve	fMRI+
M	23	4	TBI	MCS	7	SMA +ve	no evidence	fMRI+
F	70	11	Cerebral bleed	MCS	9	no evidence	no evidence	fMRI-
F	30	6	Anoxic	MCS-	9	PMC +ve	no evidence	fMRI+
F	36	6	Anoxic	UWS	8	no evidence	PPA +ve	fMRI+
M	22	5	Anoxic	UWS	7	no evidence	no evidence	fMRI-
M	40	14	Anoxic	UWS	7	no evidence	no evidence	fMRI-
F	62	7	Anoxic	UWS	7	no evidence	no evidence	fMRI-
M	46	10	Anoxic	UWS	5	no evidence	no evidence	fMRI-
M	21	7	TBI	MCS	11	no evidence	no evidence	fMRI-
M	67	14	TBI	MCS-	11	SMA +ve	PPA +ve	fMRI+
F	55	6	Hypoxia	UWS	12	negative	negative	fMRI-
M	28	14	TBI	MCS	8	positive	positive	fMRI+
M	22	12	TBI	MCS	10	negative	negative	fMRI-
F	28	8	ADEM	UWS	6	negative	negative	fMRI-

CRS-R, Coma Recovery Scale-Revised; UWS, Unresponsive Wakefulness Syndrome; MCS, Minimally Conscious State; TBI, Traumatic Brain Injury; fMRI-, negative responders to mental imagery task; fMRI+, positive responders to mental imagery task; SMA, supplementary motor area; PPA, parahippocampal place area; PMC, pre-motor cortex.

Stratification of DOC Patients into fMRI+ and fMRI-

Patients were stratified into two groups based on their ability to perform volitional tasks (mental imagery) in the scanner. The mental imagery tasks used here have been previously used to assess the presence of covert consciousness in DOC patients [25,26] and their validity has been confirmed in healthy individuals [46].

Patients were instructed to perform two mental imagery tasks. The first task involved motor imagery ("tennis task"): each patient was asked to imagine being on a tennis court swinging their arm to hit the ball back and forth with an imagined opponent. The second was a task of spatial imagery ("navigation task"): the patient was required to imagine walking around the rooms of their house, or the streets of a familiar city, and to visualise what they would see if they were there. Each task comprised five cycles of alternating imagery and rest blocks, each lasting 30 seconds. The two kinds of mental imagery blocks were cued with the spoken word "tennis" or "navigation", respectively, whereas the resting blocks were cued with the word "relax", corresponding to instructions for the patient to just stay still and keep their eyes closed.

Univariate fMRI analysis was conducted on all 22 patients for both the motor and spatial mental imagery tasks. The analyses were performed using FSL version 5.0.9 (https://fsl.fmrib.ox.ac.uk/fsl/fslwiki/). The results of these analyses determined which patients would be placed in each classification condition. For each functional scan, a general linear model consisting of contrasting periods of rest and active imagery was computed. Results were considered significant at a cluster level of $z > 2.3$ (corrected $p < 0.05$) [26].

Patients who exhibited significantly greater brain activation during either of the volitional mental imagery tasks than rest (i.e. those who exhibited evidence of being able to respond to the task) were deemed to be covertly conscious (N = 8); for brevity, we refer to these positive responders as "fMRI+". Conversely, we refer to patients who did not respond to either task (negative responders), and who therefore did not exhibit detectable evidence of covert consciousness (N = 14), as "fMRI-". (Table 1).

Resting-state FMRI Data Acquisition

Resting-state fMRI was acquired for 10 minutes (300 volumes, TR=2000ms) using a Siemens Trio 3T scanner (Erlangen, Germany). Functional images (32 slices) were acquired using an echo planar sequence, with the following parameters: 3 x 3 x 3.75mm resolution, TR = 2000ms, TE = 30ms, 78 degrees FA. Anatomical scanning was also performed, acquiring high-resolution T1-weighted images with an MPRAGE sequence, using the following parameters: TR = 2300ms, TE = 2.47ms, 150 slices, resolution 1 x 1 x 1mm.

rsfMRI Preprocessing and Denoising

Due to the presence of deformations caused by brain injury, rather than relying on automated pipelines, patients' brains were individually preprocessed using SPM12, with visual inspections after each step. Additionally, to further reduce potential movement artifacts, data underwent despiking with a hyperbolic tangent squashing function. The remaining preprocessing and denoising steps were the same as described above for the ketamine and propofol data.

LSD Dataset

Recruitment

This study was approved by the National Research Ethics Service Committee London–West London and was conducted in accordance with the revised declaration of Helsinki (2000), the International Committee on Harmonization Good Clinical Practice guidelines and National Health Service Research Governance Framework. Imperial College London sponsored the research, which was conducted under a Home Office license for research with schedule 1 drugs.

All participants were recruited via word of mouth and provided written informed consent to participate after study briefing and screening for physical and mental health. The screening for physical health included electrocardiogram (ECG), routine blood tests, and urine test for recent drug use and pregnancy. A psychiatric interview was conducted and participants provided full disclosure of their drug use history. Key exclusion criteria included: < 21 years of age, personal history of diagnosed psychiatric illness, immediate family history of a psychotic disorder, an absence of previous experience with a classic psychedelic drug (e.g. LSD, mescaline, psilocybin/magic mushrooms or DMT/ayahuasca), any psychedelic drug use within 6 weeks of the first scanning day, pregnancy, problematic alcohol use (i.e. > 40 units consumed per week), or a medically significant condition rendering the volunteer unsuitable for the study.

LSD Infusion Protocol

The data acquisition protocols were described in detail in a previous paper [47], so we will describe them in brief here. Twenty healthy volunteers with a previous experience using psychedelic drugs were scanned. Patients underwent two scans, 14 days apart. On one day they were given a placebo (10-mL saline) and the other they were given an active dose of LSD (75 μg of LSD in 10-mL saline). The infusion (drug/placebo) was administered over 2 min and occurred 115min before the resting-state scans were initiated. After infusion, subjects had a brief acclimation period in a mock MRI scanner to prepare them for the experience of being in the real machine. ASL and BOLD scanning consisted of three seven-minute eyes closed resting state scans.

FMRI Data Acquisition

The first and third scans were eyes-closed, resting state without stimulation, while the

second scan involved listening to music; however, this scan was not used in this analysis. The precise length of each of the two BOLD scans included here was 7:20 minutes. Imaging was performed on a 3T GE HDx system. High-resolution anatomical images were acquired with 3D fast spoiled gradient echo scans in an axial orientation, with field of view = 256x256x192 and matrix = 256x256x129 to yield 1mm isotropic voxel resolution. TR/TE = 7.9/3.0ms; inversion time = 450ms; flip angle = 20.

BOLD-weighted fMRI data were acquired using a gradient echo planer imaging sequence, TR/TE = 2000/35ms, FoV = 220mm, 64x64 acquisition matrix, parallel acceleration factor = 2, 90 flip angle. Thirty five oblique axial slices were acquired in an interleaved fashion, each 3.4mm thick with zero slice gap (3.4mm isotropic voxels). One subject aborted the experiment due to anxiety and four others we excluded for excessive motion (measured in terms of frame-wise displacement), leaving 15 subjects for analysis (11 males, 4 females; mean age 30.5 years, SD = 8.0 years) [47].

Preprocessing and Denoising

The same preprocessing and denoising procedures were followed as for the previous datasets.

Connectome Harmonic Decomposition

Theoretical background

The core technique employed here relies on the recently developed framework of connectome harmonic decomposition (CHD)[9,13]. This technique allows patterns of brain activity derived from functional MRI over time to be decomposed into a linear combination of a finite number of orthogonal, synchronous brain states, the harmonic modes of the human structural connectome (i.e. the network of anatomical connections between brain regions).

Each of these elementary brain states, also referred to as a connectome harmonics, is a pattern of synchronised cortical activity associated with a specific spatial frequency (i.e. granularity), corresponding to an intrinsic spatial wavenumber, *k*. Connectome harmonic decomposition may

therefore be seen as an extension of the well-known Fourier transform to the human connectome, since the Fourier transform is a special case of harmonic mode decomposition applied to a 1D domain with cyclic boundary conditions. Crucially, however, it is important to note that the frequencies associated with each connectome harmonic are in the spatial rather than temporal domain, and should not be confused with the frequencies identified by Fourier transform in the temporal domain (e.g. for denoising of timeseries).

Construction of structural connectome

In order to identify the harmonic modes of the human structural connectome, which form the basis function for our connectome harmonic decomposition of functional MRI data, we began by constructing a network of anatomical connectivity between brain regions. To this end, we used DTI and MRI data from an independent sample of 10 subjects from the Human Connectome Project (HCP; Principal Investigators: David Van Essen and Kamil Ugurbil; 1U54MH091657, funded by the 16 NIH Institutes and Centers that support the NIH Blueprint for Neuroscience Research and by the McDonnell Center for Systems Neuroscience at Washington University; https://db.humanconnectome.org). The workflow was the same as described in previous work by Atasoy and colleagues [9,13].

Freesurfer (http://freesurfer.net) was used to reconstruct the cortical surfaces at the interface of white and grey matter based on the 0.7-mm resolution data from T1-weighted MRI. This resulted in a network representation of 20,484 nodes (10,242 nodes per hemisphere) for each subject. Subsequently, deterministic tractography was used to reconstruct cortico-cortical and thalamo-cortical white matter fibres. After coregistering each subject's DTI and cortical surface data, each of the 20,484 nodes of the reconstructed cortical surface network was used as a centre to initialise eight seeds for deterministic tractography, implemented with the MrDiffusion tool (http://white.stanford.edu/newlm/index.php/MrDiffusion). Tracking was terminated when fractional anisotropy (FA) was below a threshold of 0.3, with 20mm minimum tract length, and setting 30 degrees as the maximum allowed angle between consecutive tracking steps.

Extraction of connectome harmonics

The structural connectome of each subject was represented as a binary adjacency matrix *A*, such that for each pair *i* and *j* of the n = 20,484 surface grey matter nodes, A_{ij} was set to 1 if a white matter tract existed connecting them or if they were adjacent in the gray matter cortical surface representation, and 0 otherwise, thereby yielding a symmetric (undirected) binary matrix[13]. The individual adjacency matrices were then averaged across the 10 subjects to obtain a group average matrix $\bar{A}$. We then define the degree matrix D of the graph as:

$$D(i,i) = \sum_{j=1}^{n} \bar{A}(i,j). \quad (1)$$

Following[13,48], we compute the symmetric graph Laplacian Δ_G on the group-average adjacency matrix $\bar{A}$ that represents the human connectome, in order to estimate the connectome Laplacian (discrete counterpart of the Laplace operator Δ[48] applied to the network of human structural brain connectivity):

$$\Delta_G = D^{-1/2} L D^{-1/2}, \text{with } L = D - \bar{A}. \quad (2)$$

We then calculate the connectome harmonics φ_k, $k \in \{1, \ldots, 18{,}715\}$ by solving the following eigenvalue problem:

$$\Delta_G \varphi_k(v_i) = \lambda_k \varphi_k(v_i) \; \forall v_i \in V, \qquad \text{with } 0 < \lambda_1 < \lambda_2 < .. < \lambda_n, \quad (3)$$

where λ_k, $k \in \{1, \ldots, n\}$ is the corresponding eigenvalue of the eigenfunction φ_k , V is the set of cortical surface vertices and n represents the number of vertices. In other words, λ_k and φ_k are the eigenvalues and eigenvectors of the Laplacian of the human structural connectivity network, respectively. Therefore, if φ_k is the connectome harmonic pattern of the k^{th} spatial frequency, then the corresponding eigenvalue λ_k is a term relating to the intrinsic energy of the that particular harmonic mode.

Connectome-harmonic decomposition of fMRI data.

At each timepoint $t \in \{1,\ldots,T\}$ (corresponding to one TR), the fMRI data were projected onto cortical surface coordinates by means of the Human Connectome Project Workbench -*volume-to-*

surface-mapping tool. Then, the spatial pattern of cortical activity over vertices *v* at time *t*, denoted as $F_t(v)$, was decomposed as a linear combination of the set of connectome harmonics $\Psi = \{\varphi_k\}_{k=1}^{N}$:

$$F_t = \omega_1(t)\varphi_1 + \omega_2(t)\varphi_2 + \ldots + \omega_n(t)\varphi_n = \sum_{k=1}^{n} \omega_k(t)\varphi_k(v) \quad (4)$$

with the contribution $\omega_k(t)$ of each connectome harmonic φ_k at time *t* being estimated as the projection (dot product) of the fMRI data $F_t(v)$ onto φ_k:

$$\omega_k(t) = \langle F_t, \varphi_k \rangle. \quad (5)$$

Power and Energy of connectome harmonics

Once the fMRI cortical activation pattern at time *t* has been decomposed into a linear combination of connectome harmonics, the magnitude of contribution to cortical activity of each harmonic φ_k, $k \in \{1, \ldots, n\}$ (regardless of sign) at any given timepoint t ($P(\varphi_k, t)$), called its "power" for analogy with the Fourier transform, is computed as the amplitude of its contribution:

$$P(\varphi_k, t) = |\omega_k(t)|. \quad (6)$$

In turn, the normalized frequency-specific contribution of each harmonic φ_k, $k \in \{1, \ldots, n\}$ at timepoint *t*, termed "energy", is estimated by combining the strength of activation (power) of a particular connectome harmonic with its own intrinsic energy given by ${\lambda_k}^2$:

$$E(\varphi_k, t) = |\omega_k(t)|^2 {\lambda_k}^2. \quad (7)$$

Consequently, total brain energy at time *t* is given by

$$E_{total}(t) = \sum_{k=1}^{n} |\omega_k(t)|^2 \lambda_k{}^2 = \|\Delta F_t(v)\|^2. \quad (8)$$

Since the Laplace operator Δ represents the amount of activity flow, the latter part of Equation 8 indicates that the total brain energy at a given point in time can be interpreted as the total cortical flow of neural activity at that time[9].

Data-driven extraction of multivariate energy signatures

Partial least squares (PLS, also known as Projection on Latent Spaces) is a multivariate statistical analysis used to identify relationships between sets of variables X (predictors) and Y (targets), in order to extract principal components as linear combinations of variables in each set that maximally covary with each other [34]. In the present case, for each pair of states of consciousness under comparison, X was the matrix of 15 binned energy values per subject (averaged over timepoints) , and Y was the vector of binary classification between the two states (here, target vs baseline state of consciousness, e.g. anaesthetised vs awake, ketamine vs placebo, fMRI- vs fMRI+ DOC, etc) – making this an application of Partial Least Squares Discriminant Analysis (PLS-DA), owing to the binary nature of Y[49].

The first principal component extracted by PLS-DA represents the single most discriminative pattern present in the data, in terms of distinguishing observations (subjects) belonging to the two different classes (states of consciousness). Here, we refer to this pattern as the "multivariate signature" (MVS).

To determine the cross-dataset generalisability of multivariate signatures, we selected four source MVSs: one from the contrast between awake and moderate propofol anaesthesia; one from the contrast between fMRI+ and fMRI- DOC patients; one from the contrast between placebo and ketamine; and one from the contrast between placebo and LSD. For each subject and condition, each source MVS was projected onto the pattern of binned connectome harmonic energy at each timepoint, by taking their dot product. The result is a measure of the match between the relevant

multivariate signature and the harmonic energy, for each timepoint of each subject, which can then be compared across states of consciousness.

Diversity of connectome harmonic repertoire

To quantify the diversity of the repertoire of connectome harmonics recruited at each point in time, we start by observing that a diverse repertoire is one in which different harmonic modes contribute in different degrees to brain activity – neither one single mode dominating (which would correspond to a periodic oscillation) nor every mode contributing the same as every other mode (which would correspond to white noise). To capture this intuition, we quantify repertoire diversity in terms of the entropy of the distribution of connectome harmonic power (absolute strength of contribution to the cortical activation pattern) at each timepoint, which we calculate for each timepoint of each subject.

Specifically, to deal with continuous data (as in the present case) we rely on the Kozachenko approximation, as implemented in the Java Information Dynamics Toolbox (JIDT; http://jlizier.github.io/jidt/)[50]. We note that when dealing with continuous variables, entropy can have negative values[51], but its interpretation remains the same: a more entropic distribution (i.e. having a value of entropy closer to positive infinity) will correspond to a more diverse repertoire.

Statistical Analysis

Linear Mixed Effects models (implemented as the MATLAB function *fitlme*) were used to assess the statistical significance of the differences between conditions (states of consciousness), treating condition as a fixed effect, and subjects as random effects. When one measurement was obtained for each timepoint, timepoints were also included as random effects, nested within subjects. Results are reported in terms of the fixed effect of condition, and the upper and lower bounds of its 95% confidence interval, with associated p-value. For comparison of frequency-specific harmonic energy, the False Discovery Rate for multiple comparisons across 15 frequency bins was controlled by means of the Benjamini-Hochberg procedure [52].

Acknowledgements

AIL, JV and PAMM would like to thank Lena Dorfschmidt for co-organising OxBridge BrainHack 2019, where this work began. We also thank all volunteers and patients who provided data.

Funding: This work was supported by grants from the UK Medical Research Council (U.1055.01.002.00001.01) [JDP]; The James S. McDonnell Foundation [JDP]; The Canadian Institute for Advanced research (CIFAR) [DKM and EAS]; The National Institute for Health Research (NIHR, UK), Cambridge Biomedical Research Centre and NIHR Senior Investigator Awards [JDP and DKM]; The British Oxygen Professorship of the Royal College of Anaesthetists [DKM]; The Stephen Erskine Fellowship, Queens' College, University of Cambridge [EAS]; The Evelyn Trust, Cambridge and the EoE CLAHRC fellowship [JA]; The Gates Cambridge Trust [AIL]; The Cambridge International Trust and the Howard Sidney Sussex Studentship [MMC]; The Oon Khye Beng Ch'Hia Tsio Studentship for Research in Preventive Medicine, Downing College, University of Cambridge [IP]; The Wellcome Trust (grant no. 210920/Z/18/Z) [PAMM]; The European Research Council Consolidator Grant CAREGIVING (615539) [MLK and SA]; The Center for Music in the Brain, funded by the Danish National Research Foundation (DNRF117) [MLK, SA and JV]; The Centre for Eudaimonia and Human Flourishing, funded by the Pettit and Carlsberg Foundations [MLK]; The Imperial College President's Scholarship [LR]; The Alex Mosley Charitable Trust [RLCH]; The Wellcome Trust Research Training Fellowship (grant no. 083660/Z/07/Z), Raymond and Beverly Sackler Studentship, and the Cambridge Commonwealth Trust [RA]. The ketamine study was funded by the Bernard Wolfe Health Neuroscience Fund and the Wellcome Trust. The original LSD study received support from a Crowd Funding Campaign and the Beckley Foundation, as part of the Beckley-Imperial Research Programme. The research was also supported by the NIHR Brain Injury Healthcare Technology Co-operative based at Cambridge University Hospitals NHS Foundation Trust and University of Cambridge. Data used to obtain the human connectome were provided by the Human Connectome Project, WU-Minn Consortium (Principal Investigators: David Van Essen and Kamil Ugurbil; 1U54MH091657) funded by the 16 NIH Institutes and Centers that support the NIH Blueprint for

Neuroscience Research; and by the McDonnell Center for Systems Neuroscience at Washington University.

Author contributions: AIL, JV, EAS, SA and MLK conceived the study. AIL, JV, PAMM, SA, MLK and EAS designed the methodology and the analysis. AIL analysed the data. JV, PAMM, MMC, and IP contributed to data analysis. PF, GBW, JA, JDP, RA, DKM, EAS, LR, RLCH were involved in designing the original studies for which the present data were collected. PF, MMC, GBW, JA, EAS, RA, RLCH, LR all participated in data collection. AIL, EAS and SA wrote the manuscript with feedback from all co-authors.

Conflicts of interest: the authors declare that no conflicts of interest exist.

Data and materials availability. The datasets analysed during the current study can be made available on request. The CONN toolbox is freely available online (http://www.nitrc.org/projects/conn). The Java Information Dynamics Toolbox is freely available online: https://github.com/jlizier/jidt.

REFERENCES

1. Northoff, G., Wainio-Theberge, S. & Evers, K. Is temporo-spatial dynamics the common currency of brain and mind? In Quest of Spatiotemporal Neuroscience. (2019). doi:10.1016/j.plrev.2019.05.002
2. Demertzi, A. *et al.* Human consciousness is supported by dynamic complex patterns of brain signal coordination. *Sci. Adv.* **5**, 1–12 (2019).
3. Luppi, A. I. *et al.* Consciousness-specific dynamic interactions of brain integration and functional diversity. *Nat. Commun.* (2019).
4. Cao, B. *et al.* Abnormal dynamic properties of functional connectivity in disorders of consciousness. *NeuroImage Clin.* **24**, (2019).
5. Lord, L. D. *et al.* Dynamical exploration of the repertoire of brain networks at rest is modulated by psilocybin. *Neuroimage* **199**, 127–142 (2019).
6. Barttfeld, P. *et al.* Signature of consciousness in the dynamics of resting-state brain activity. *Proc. Natl. Acad. Sci.* **112**, 887–892 (2015).
7. Varley, T. F. *et al.* Consciousness & Brain Functional Complexity in Propofol Anaesthesia. *Sci. Rep.* **10**, (2020).
8. Atasoy, S., Deco, G., Kringelbach, M. & Pearson, J. Harmonic Brain Modes: A Unifying Framework for Linking Space and Time in Brain Dynamic. *Neurosci.* (2018).

doi:10.1177/1073858417728032

9. Atasoy, S. *et al.* Connectome-harmonic decomposition of human brain activity reveals dynamical repertoire re-organization under LSD. *Sci. Rep.* **7**, 1–18 (2017).
10. Atasoy, S., Vohryzek, J., Deco, G., Carhart-harris, R. L. & Kringelbach, M. L. Common neural signatures of psychedelics: Frequency-specific energy changes and repertoire expansion revealed using connectome-harmonic decomposition. **242**, (2018).
11. Wang, M. B., Owen, J. P., Mukherjee, P. & Raj, A. Brain network eigenmodes provide a robust and compact representation of the structural connectome in health and disease. *PLoS Comput. Biol.* **13**, (2017).
12. Murray, J. D. *Mathematical Biology II - Spatial Models and Biomedical Applications*. *Mathematical Biology II - Spatial Models and Biomedical Applications* (Springer, 2008). doi:10.1007/b98869
13. Atasoy, S., Donnelly, I. & Pearson, J. Human brain networks function in connectome-specific harmonic waves. *Nat. Commun.* **7**, (2016).
14. Gabay, N. C. & Robinson, P. A. Cortical geometry as a determinant of brain activity eigenmodes: Neural field analysis. *Phys. Rev. E* **96**, 32413 (2017).
15. Carhart-Harris, R. L. *et al.* The entropic brain: a theory of conscious states informed by neuroimaging research with psychedelic drugs. *Front. Hum. Neurosci.* **8**, 20 (2014).
16. Carhart-Harris, R. L. & Friston, K. J. REBUS and the anarchic brain: Toward a unified model of the brain action of psychedelics. *Pharmacol. Rev.* **71**, 316–344 (2019).
17. Schartner, M. M., Carhart-Harris, R. L., Barrett, A. B., Seth, A. K. & Muthukumaraswamy, S. D. Increased spontaneous MEG signal diversity for psychoactive doses of ketamine, LSD and psilocybin. *Sci. Rep.* **7**, 46421 (2017).
18. Schartner, M. *et al.* Complexity of multi-dimensional spontaneous EEG decreases during propofol induced general anaesthesia. *PLoS One* **10**, (2015).
19. Schartner, M. M. *et al.* Global and local complexity of intracranial EEG decreases during NREM sleep. *Neurosci. Conscious.* (2017). doi:10.1093/nc/niw022
20. Sarasso, S. *et al.* Consciousness and Complexity during Unresponsiveness Induced by Propofol, Xenon, and Ketamine. *CURBIO* **25**, 3099–3105 (2015).
21. Li, D. & Mashour, G. A. Cortical dynamics during psychedelic and anesthetized states induced by ketamine. *Neuroimage* **196**, 32–40 (2019).
22. Bayne, T. & Carter, O. Dimensions of consciousness and the psychedelic state. *Neurosci. Conscious.* **2018**, (2018).
23. Stamatakis, E. A., Adapa, R. M., Absalom, A. R. & Menon, D. K. Changes in resting neural connectivity during propofol sedation. *PLoS One* **5**, e14224 (2010).
24. Brown, E. N., Lydic, R. & Schiff, N. D. General Anesthesia, Sleep, and Coma. *N. Engl. J. Med.* **27**, 2638–50 (2010).
25. Owen, A. M. *et al.* Detecting awareness in the vegetative state. *Science (80-.).* **313**, 1402 (2006).
26. Monti, M. M. *et al.* Willful modulation of brain activity in disorders of consciousness. *N. Engl. J. Med.* **362**, 579–589 (2010).
27. Radtke, F. M. *et al.* Risk factors for inadequate emergence after anesthesia: Emergence delirium and hypoactive emergence. *Minerva Anestesiol.* **76**, 394–404 (2010).
28. Xará, D., Silva, A., Mendonça, J. & Abelha, F. Inadequate emergence after anesthesia: emergence delirium and hypoactive emergence in the Postanesthesia Care Unit. *J. Clin. Anesth.* **25**, 439–446 (2013).

29. Dandash, O. *et al.* Selective Augmentation of Striatal Functional Connectivity Following NMDA Receptor Antagonism: Implications for Psychosis. *Neuropsychopharmacology* **40**, 622–631 (2015).
30. Olney, J. W., Newcomer, J. W. & Farber, N. B. NMDA receptor hypofunction model of schizophrenia. *J. Psychiatr. Res.* **33**, 523–533 (1999).
31. Corlett, P. R., Honey, G. D. & Fletcher, P. C. Prediction error, ketamine and psychosis: An updated model. *J. Psychopharmacol.* **30**, 1145–1155 (2016).
32. Carhart-Harris, R. L., Brugger, S., Nutt, D. J. & Stone, J. M. Psychiatry's next top model: Cause for a re-think on drug models of psychosis and other psychiatric disorders. *J. Psychopharmacol.* **27**, 771–778 (2013).
33. Preti, M. G. & Van De Ville, D. Decoupling of brain function from structure reveals regional behavioral specialization in humans. *Nat. Commun.* **10**, (2019).
34. Krishnan, A., Williams, L. J., McIntosh, A. R. & Abdi, H. Partial Least Squares (PLS) methods for neuroimaging: A tutorial and review. *Neuroimage* **56**, 455–475 (2011).
35. Scott, G. & Carhart-Harris, R. L. Psychedelics as a treatment for disorders of consciousness. *Neurosci. Conscious.* **2019**, niz003 (2019).
36. Huang, Z. *et al.* Brain imaging reveals covert consciousness during behavioral unresponsiveness induced by propofol. *Sci. Rep.* **8**, 1–11 (2018).
37. Ní Mhuircheartaigh, R., Warnaby, C., Rogers, R., Jbabdi, S. & Tracey, I. Slow-wave activity saturation and thalamocortical isolation during propofol anesthesia in humans. *Sci. Transl. Med.* **5**, 208ra148 (2013).
38. Leslie, K. *et al.* Dreaming and Electroencephalographic Changes during Anesthesia Maintained with Propofol or Desflurane. *Anesthesiology* **111**, 547–555 (2009).
39. Naci, L., Sinai, L. & Owen, A. M. Detecting and interpreting conscious experiences in behaviorally non-responsive patients. *Neuroimage* (2015). doi:10.1016/j.neuroimage.2015.11.059
40. Casali, A. G. *et al.* A Theoretically Based Index of Consciousness Independent of Sensory Processing and Behavior. in *Science translational medicine* **5**, 1–10 (2013).
41. Corlett, P. R. *et al.* Frontal responses during learning predict vulnerability to the psychotogenic effects of ketamine: Linking cognition, brain activity, and psychosis. *Arch. Gen. Psychiatry* **63**, 611–621 (2006).
42. Whitfield-Gabrieli, S. & Nieto-Castanon, A. Conn: A Functional Connectivity Toolbox for Correlated and Anticorrelated Brain Networks. *Brain Connect.* **2**, 125–141 (2012).
43. Behzadi Y, Restom K, Liau J & Liu TT. A component based noise correction method (CompCor) for BOLD and perfusion based fMRI. *Neuroimage* **37**, 90–101 (2007).
44. Bruno, M.-A., Vanhaudenhuyse, A., Thibaut, A., Moonen, G. & Laureys, S. From unresponsive wakefulness to minimally conscious PLUS and functional locked-in syndromes: recent advances in our understanding of disorders of consciousness. *J. Neurol.* **258**, 1373–1384 (2011).
45. Wannez, S. *et al.* Prevalence of coma-recovery scale-revised signs of consciousness in patients in minimally conscious state. *Neuropsychol. Rehabil.* **28**, 1350–1359 (2018).
46. Fernández-Espejo, D., Norton, L. & Owen, A. M. The clinical utility of fMRI for identifying covert awareness in the vegetative state: A comparison of sensitivity between 3T and 1.5T. *PLoS One* **9**, (2014).
47. Carhart-Harris, R. L. *et al.* Neural correlates of the LSD experience revealed by multimodal neuroimaging. *Proc. Natl. Acad. Sci.* **113**, 201518377 (2016).

48. Chung, F. *Spectral Graph Theory*. (American Mathematical Society, 1997).
49. Chuen Lee, L., Liong, C.-Y. & Aziz Jemain, A. Partial least squares-discriminant analysis (PLS-DA) for classification of high-dimensional (HD) data: a review of contemporary practice strategies and knowledge gaps †. *Analyst* **143**, 3526 (2018).
50. Lizier, J. T. JIDT: An Information-Theoretic Toolkit for Studying the Dynamics of Complex Systems. *Front. Robot. AI* **1**, 1–37 (2014).
51. Cover, T. M. & Thomas, J. A. *Elements of Information Theory*. *Elements of Information Theory* (Wiley-Interscience, 2005). doi:10.1002/047174882X
52. Banjamini, Y. & Hochberg, Y. Controlling the False Discovery Rate: A Practical and Powerful Approach to Multiple Testing. *J. R. Stat. Soc. Ser. B* **57**, 289–300 (1995).

Supplementary Information for:

Connectome Harmonic Decomposition of Human Brain Dynamics Reveals a Landscape of Consciousness

Luppi A.I. [a,b]*, Vohryzek J. [c,d], Kringelbach M. L.[c,d], Mediano P.A.M. [e], Craig M. M. [a,b], Adapa R. [a], Carhart-Harris, R. L. [f], Roseman, L. [f], Pappas I. [a,b,g], Finoia P. [a,h], Williams G. B. [b,i], Allanson J. [b,j], Pickard J. D. [b,h,i], Menon D. K. [a], Atasoy S. [c,d], & Stamatakis E.A. [a,b]

Supplementary Figures

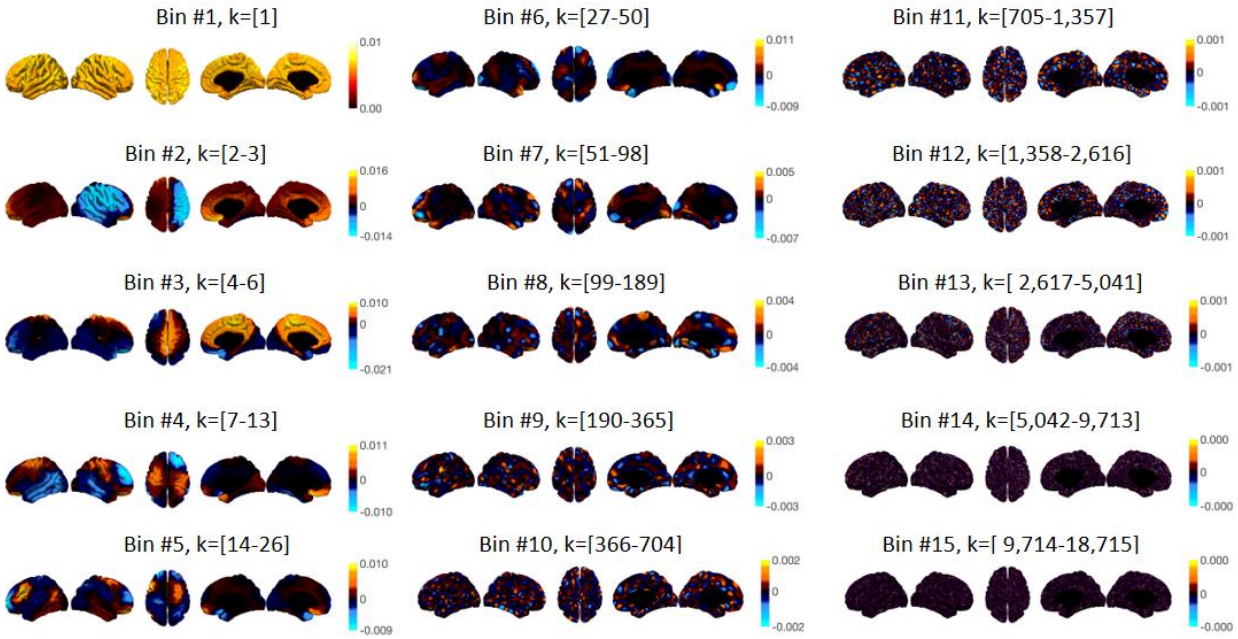

Supplementary Figure 1. **Binned connectome harmonics**. Surface projections of connectome harmonics averaged over each of 15 logarithmically spaced bins (with corresponding wavenumbers *k* indicated in braces), showing the progressive increase in complexity and granularity of the connectome harmonic patterns, with increasing spatial frequency.

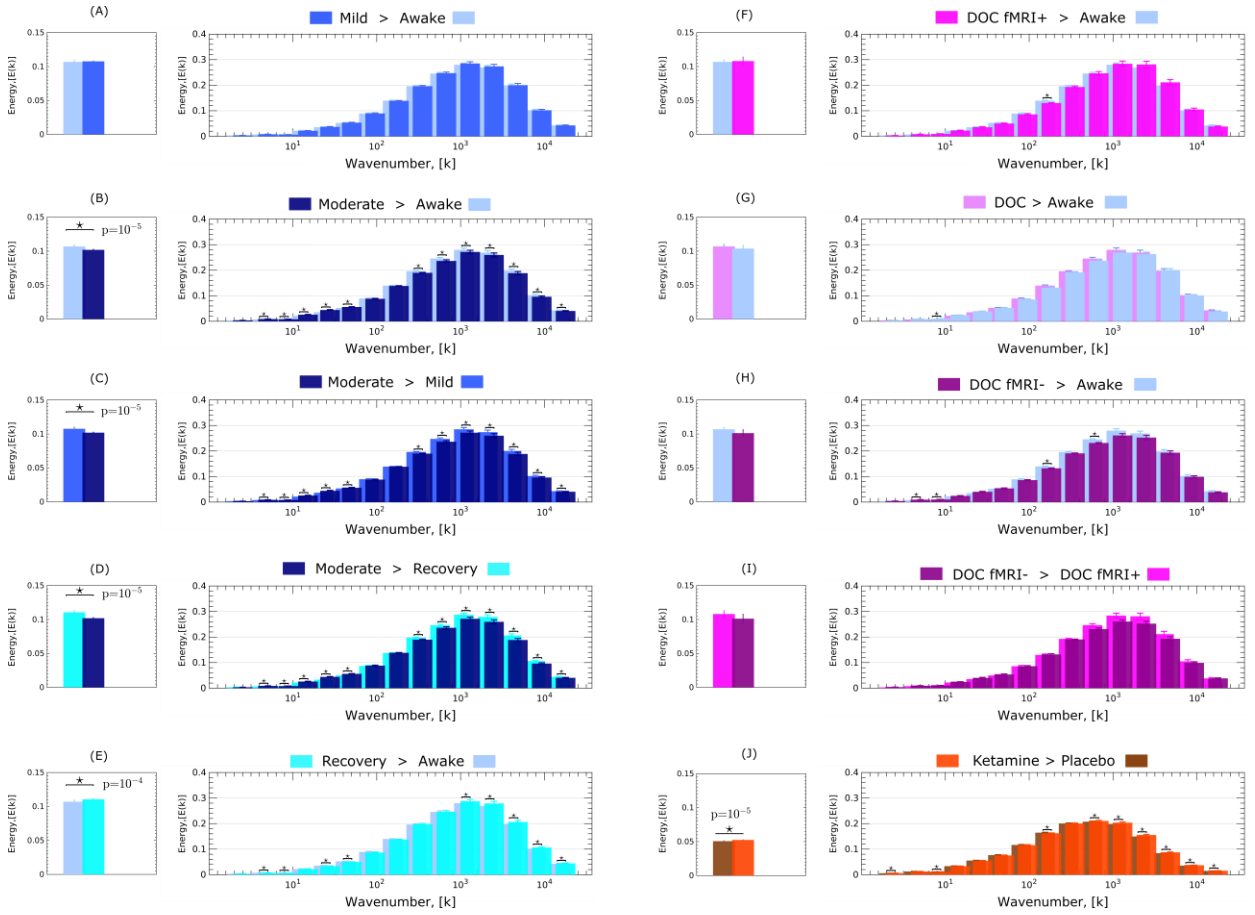

Supplementary Figure 2. **Energy levels across states of consciousness**. (a) Total energy (left) and frequency-specific energy of connectome harmonics (right) for Mild propofol sedation vs wakefulness. (b) Total energy (left) and frequency-specific energy of connectome harmonics (right) for Moderate anaesthesia vs wakefulness. (c) Total energy (left) and frequency-specific energy of connectome harmonics (right) for Moderate anaesthesia vs mild sedation. (d) Total energy (left) and frequency-specific energy of connectome harmonics (right) for Moderate anaesthesia vs post-anaesthetic recovery. (e) Total energy (left) and frequency-specific energy of connectome harmonics (right) for Recovery vs wakefulness. (f) Total energy (left) and frequency-specific energy of connectome harmonics (right) for DOC patients vs awake healthy controls. (g) Total energy (left) and frequency-specific energy of connectome harmonics (right) for DOC fMRI+ patients vs awake healthy controls. (h) Total energy (left) and frequency-specific energy of connectome harmonics (right) for DOC fMRI- patients vs awake healthy controls. (i) Total energy (left) and frequency-specific energy of connectome harmonics (right) for fMRI- vs fMRI+ DOC patients. (j) Ketamine > placebo. * $p < 0.05$ (FDR-corrected across 15 frequency bins, for the frequency-specific analysis).

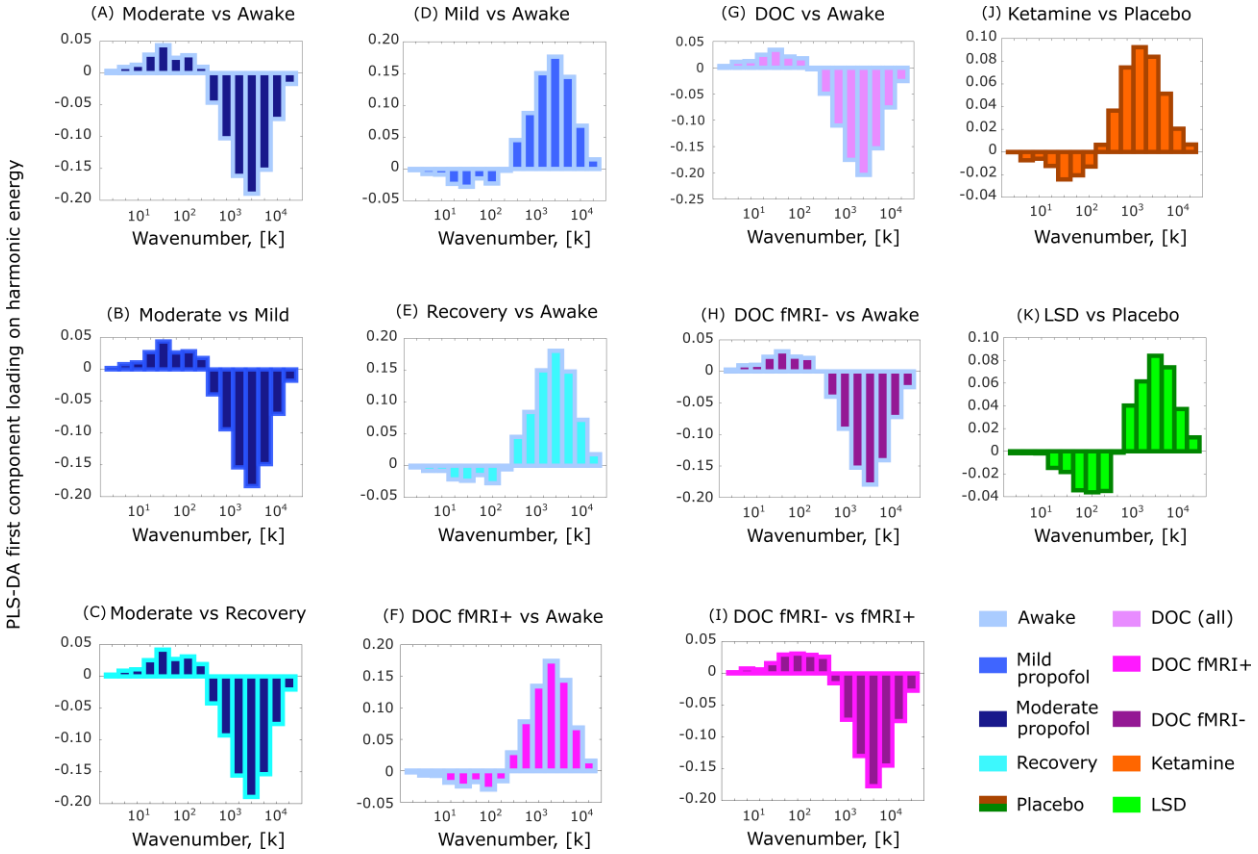

Supplementary Figure 3. Similarity of PLS-DA maximally discriminative components of connectome harmonic energy between states of consciousness. (a) Moderate anaesthesia > wakefulness. (b) Moderate anaesthesia > mild sedation. (c) Moderate anaesthesia > post-anaesthetic recovery. (d) Mild sedation > wakefulness. (e) Post-anaesthetic recovery > wakefulness. (f) DOC fMRI+ patients > awake healthy controls. (g) DOC patients > awake healthy controls. (h) DOC fMRI- patients > awake healthy controls. (i) fMRI- > fMRI+ DOC patients. (j) Ketamine > placebo. (k) LSD > placebo. Bar colour indicates the target state; contours indicate the reference state.

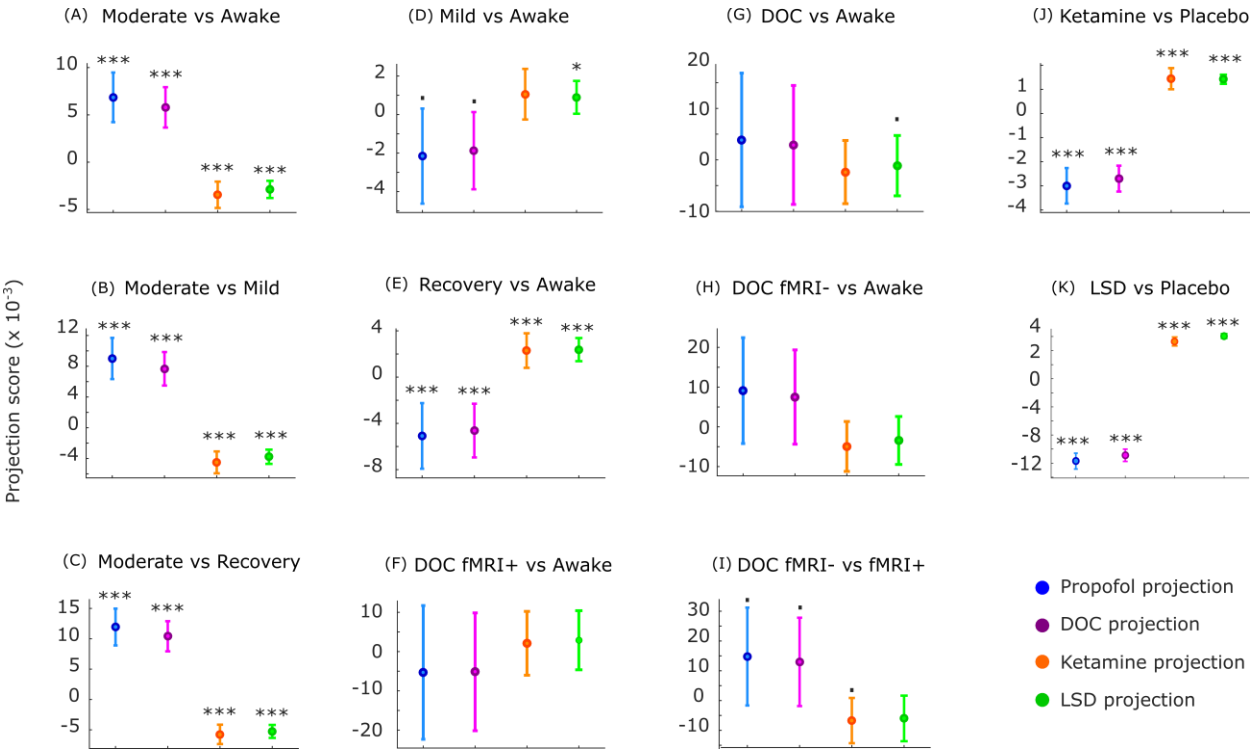

Supplementary Figure 4. Maximally discriminative patterns of connectome harmonic energy are generalisable across states of consciousness. Each panel shows the fixed effects (and 95% CI) of contrasting the projections (dot product) of MDC patterns from four source states (moderate propofol anaesthesia, DOC patients, ketamine and LSD) onto each pair of the states of consciousness under comparison. (a) Moderate anaesthesia > wakefulness. (b) Moderate anaesthesia > mild sedation. (c) Moderate anaesthesia > post-anaesthetic recovery. (d) Mild sedation > wakefulness. (e) Post-anaesthetic recovery > wakefulness. (f) DOC fMRI+ patients > awake healthy controls. (g) DOC patients > awake healthy controls. (h) DOC fMRI- patients > awake healthy controls. (i) fMRI- > fMRI+ DOC patients. (j) Ketamine > placebo. (k) LSD > placebo. * $p < 0.05$; ** $p < 0.01$; *** $p < 0.001$; . $p < 010$.

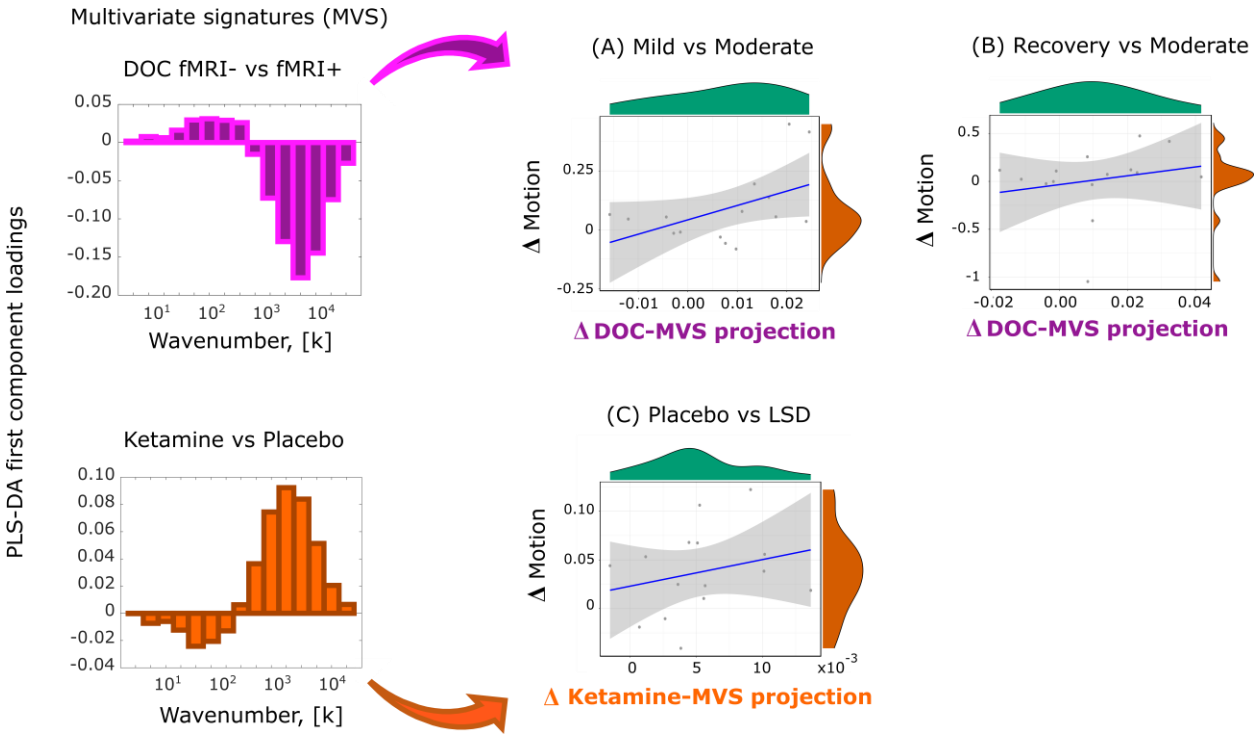

Supplementary Figure 5. Change in projection onto cross-dataset multivariate energy signature (MVS) does not significantly correlate with differences in subject motion in the scanner. (a) Scatterplot of delta in connectome harmonic energy projection onto the MVS derived from the DOC dataset, versus the delta in head motion (moderate anaesthesia minus mild anaesthesia). (b) Scatterplot of delta in connectome harmonic energy projection onto the MVS derived from the DOC dataset, versus the delta in head motion (moderate anaesthesia minus recovery). (c) Scatterplot of delta in connectome harmonic energy projection onto the MVS derived from the ketamine dataset, versus the delta in head motion (LSD minus placebo).

Supplementary Tables

Supplementary Table 1. LME results for total connectome harmonic energy (units are $x10^{-3}$). * $p < 0.05$; ** $p < 0.01$; *** $p < 0.001$; . $p < 010$; n.s. not significant.

Contrast	Fixed Effect	95% CI Lower	95% CI Upper	p-value	Significance
Awake vs fMRI-	-5.598	-15.603	4.406	0.273	n.s.
fMRI+ vs fMRI-	-6.835	-19.879	6.209	0.304	n.s.
Awake vs DOC	-3.113	-12.533	6.307	0.517	n.s.
Awake vs Moderate Propofol	-4.943	-6.593	-3.293	p < 0.001	***
Mild vs Moderate Propofol	-5.724	-7.394	-4.055	p < 0.001	***
Recovery vs Moderate Propofol	-8.665	-10.597	-6.733	p < 0.001	***
Awake vs fMRI+	1.236	-10.359	12.832	0.834	n.s.
Awake vs Mild Propofol	0.782	-0.758	2.321	0.320	n.s.
Awake vs Recovery	3.722	1.904	5.541	p < 0.001	***
Placebo vs Ketamine	1.798	1.425	2.172	p < 0.001	***
Placebo vs LSD	8.101	7.472	8.730	p < 0.001	***

Supplementary Table 2. LME results for the projection onto the PLS-DA first component of different states of consciousness (units are $x10^{-3}$). * $p < 0.05$; ** $p < 0.01$; *** $p < 0.001$; . $p < 010$; n.s. not significant.

Dataset	Source	Fixed Effect	95% CI Lower	95% CI Upper	p-value	Significance
Placebo vs LSD	propofol	-11.71	-12.84	-10.59	p < 0.001	***
	DOC	-10.88	-11.75	-10.01	p < 0.001	***
	ketamine	5.30	4.67	5.93	p < 0.001	***
	LSD	6.08	5.74	6.42	p < 0.001	***
Placebo vs Ketamine	propofol	-3.00	-3.74	-2.26	p < 0.001	***
	DOC	-2.70	-3.24	-2.16	p < 0.001	***
	ketamine	1.44	1.01	1.88	p < 0.001	***
	LSD	1.42	1.23	1.61	p < 0.001	***
Propofol Awake vs Mild	propofol	-2.16	-4.62	0.31	0.087	.
	DOC	-1.88	-3.88	0.13	0.067	.
	ketamine	1.06	-0.26	2.37	0.115	
	LSD	0.89	0.04	1.75	0.040	*
Propofol Awake vs Recovery	propofol	-5.08	-7.92	-2.25	p < 0.001	***
	DOC	-4.62	-6.94	-2.30	p < 0.001	***
	ketamine	2.30	0.80	3.79	0.003	**
	LSD	2.38	1.38	3.38	p < 0.001	***
Propofol Awake vs Moderate	propofol	6.85	4.23	9.48	p < 0.001	***
	DOC	5.79	3.66	7.93	p < 0.001	***
	ketamine	-3.45	-4.84	-2.06	p < 0.001	***
	LSD	-2.88	-3.79	-1.97	p < 0.001	***
Propofol Mild vs Moderate	propofol	9.01	6.33	11.69	p < 0.001	***

	DOC	7.67	5.49	9.85	p < 0.001	***
	ketamine	-4.51	-5.93	-3.08	p < 0.001	***
	LSD	-3.78	-4.70	-2.85	p < 0.001	***
Propofol Recovery vs Moderate	propofol	11.94	8.90	14.97	p < 0.001	***
	DOC	10.41	7.93	12.90	p < 0.001	***
	ketamine	-5.75	-7.34	-4.15	p < 0.001	***
	LSD	-5.26	-6.33	-4.19	p < 0.001	***
DOC fMRI+ vs fMRI-	propofol	14.43	-1.97	30.83	0.085	.
	DOC	12.65	-2.18	27.48	0.094	.
	ketamine	-7.04	-14.63	0.55	0.069	.
	LSD	-6.32	-13.97	1.33	0.105	
Awake vs DOC	propofol	3.87	-9.13	16.86	0.098	.
	DOC	2.90	-8.67	14.46	0.101	n.s.
	ketamine	-2.38	-8.52	3.77	0.105	n.s.
	LSD	-1.13	-7.00	4.74	0.109	n.s.
Awake vs DOC fMRI+	propofol	-5.31	-22.34	11.72	0.112	n.s.
	DOC	-5.16	-20.17	9.85	0.116	n.s.
	ketamine	2.11	-6.02	10.23	0.120	n.s.
	LSD	2.89	-4.64	10.42	0.123	n.s.
Awake vs DOC fMRI-	propofol	9.11	-4.20	22.43	0.127	n.s.
	DOC	7.50	-4.37	19.36	0.131	n.s.
	ketamine	-4.94	-11.21	1.34	0.134	n.s.
	LSD	-3.43	-9.46	2.60	0.138	n.s.

Supplementary Table 3. Correlations of cross-dataset projections onto MDCs with mean motion difference. $p < 010$; n.s. not significant.

	Spearman's ρ	CI 95%	p-value	Sig
Moderate-Mild Motion Delta vs DOC Projection Delta	0.45	[-0.08; 0.78]	0.089	.
Moderate-Recovery Motion Delta vs DOC Projection Delta	0.31	[-0.24; 0.71]	0.254	n.s.
LSD-Placebo Motion Delta vs Ketamine Projection Delta	0.24	[-0.31; 0.67]	0.383	n.s.

Supplementary Table 4. LME results for repertoire diversity of the connectome harmonics. * $p < 0.05$; ** $p < 0.01$; *** $p < 0.001$; ** $p < 0.01$; . $p < 010$; n.s. not significant.

Contrast	Fixed Effect	95% CI Lower	95% CI Upper	p-value	Significance
Awake vs fMRI-	-0.074	-0.129	-0.018	0.009	**
fMRI+ vs fMRI-	-0.063	-0.133	0.007	0.079	.
Awake vs DOC	-0.051	-0.102	0.000	0.051	.
Awake vs Moderate Propofol	-0.039	-0.052	-0.026	p < 0.001	***
Mild vs Moderate Propofol	-0.040	-0.054	-0.027	p < 0.001	***
Recovery vs Moderate Propofol	-0.040	-0.055	-0.025	p < 0.001	***
Awake vs fMRI+	-0.011	-0.064	0.042	0.691	n.s.
Awake vs Mild Propofol	0.001	-0.011	0.013	0.880	n.s.
Awake vs Recovery	0.001	-0.013	0.014	0.928	n.s.
Placebo vs Ketamine	0.020	0.016	0.024	p < 0.001	***
Placebo vs LSD	0.054	0.049	0.059	p < 0.001	***